Development, Parameterization and Verification of a Series Hybrid Vehicle Model to investigate Energy Management Strategies

Claudia Meis
Technische Universität München
Institute of Automotive Technology
Munich, Germany

Dr. Michael Lehmann*, Prof. Dr. Lienkamp[&], Prof. Dr. Spiegelberg[§]
*Siemens, Infrastructure and Cities Sector, Erlangen, Germany
[&]Technische Universität München, Institute of Automotive Technology, Munich, Germany
[§]Siemens, Corporate Technology, Munich, Germany

***Abstract*— Analyzing the impacts of an energy management strategy, simulation offers advantages over measurements on a real vehicle as it is far more cost effective and time saving. In particular, when the energy management strategy for different vehicles is analyzed under different conditions (driving profile, environmental conditions), the advantages of the simulation are significant. A vehicle model developed for this simulation serves as the basis to investigate the approach of a flexible electric energy management (FEEM) for series-hybrid trucks that was developed prior. The FEEM offers vehicle manufacturers the advantage to be used for a variety of vehicles with different electrical sources and sinks without having to be modified fundamentally. This gets more important as the variety of commercial available vehicles and the number of different assemblies of electrical sources and sinks increases. To show the energetic plug-in capability, a model of a series hybrid vehicle with various sources and sinks, which have the appropriate interfaces to the FEEM, is developed. The FEEM offers benefits to the vehicle operator, since it minimizes the total costs of the electrical sources. At the same time the priority of supplying the electrical sinks is taken into consideration for the energy distribution. Consequently, the resulting operating costs of each electrical source must be calculated within the vehicle model. In this context, not only the fuel consumption is calculated, as usual, but also other effects such as the aging of the battery, or maintenance of components are taken into account. Validity of the vehicle model has to be demonstrated before results from the simulations can be obtained. For this purpose, the vehicle model is parameterized with data of the real truck and afterwards simulation results are compared to measurements of the real truck.**

Keywords—Energy Management; Hybrid Vehicle; Modelling; Simulation

I. INTRODUCTION

In a hybrid vehicle there are electrical sources, which convert energy of another form into electric energy and electrical sinks, which use the electric energy to fulfill their function [1]. The purpose of the electric energy management is to define the amount of power for every electrical source and sink for each time step, which it should provide or gain [2]. Therefore it takes into account the driver's request, environmental data, status data of the components and pursues an optimization goal. In the commercial vehicle sector, the operating costs are crucial to the vehicle operator. Therefore, the goal of the developed energy management approach is to minimize the operating costs of the electrical sources holistically. In addition, the commercial vehicle market is characterized by a broad variety of vehicle variants. Therefore, a second goal of the developed flexible energy management (FEEM) is to have a so-called plug-in energetic capability. This occurs when energy components, i.e. electrical sources and sinks, can be integrated into the energy management system without fundamentally changing the FEEM [3]. Therefore the energy management system must be expandable and scalable. It has to be able to operate with only one source respectively one sink, but also with a large number of sources and sinks. At the same time, the characteristics of the sources and sinks may vary. For a series hybrid truck, this means for example that the maximum power of the electric motor or the battery may vary. Additionally, instead of the batteries other storages like ultracapacitors can be used, or a part of the route can be equipped with a continuous power supply, e.g. an overhead contact line system.

As described in [4], the FEEM provides a cost-power function for each energy component to enter an energy trade within the energy management. The cost-power functions are dynamically parameterized due to driver inputs, state data and environmental data. The cost-power function of an electrical source describes the correlation between operational costs and provided electric power. On the contrary, the cost-power function of an electrical sink quantifies the priority to be supplied with electric power. All cost-power functions are summed in the central energy management, as shown in 1. As a result, the market price is determined.

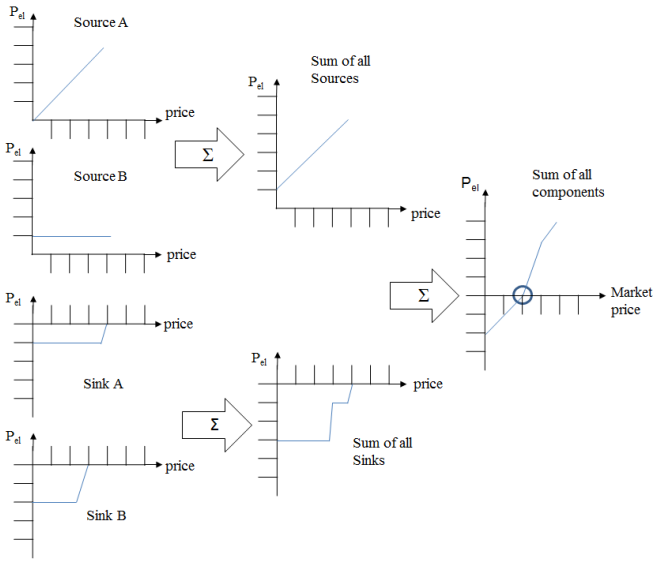

Fig. 1. Determination of the market price

Afterwards the market price and the cost-power functions of the energy components are used, to determine the power the energy components have to provide or receive (figure 2). The requirement of the energy management is implemented decentralized and independently by the energy components.

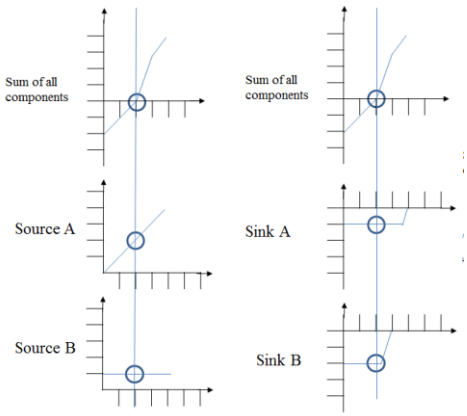

Fig. 2. Determination of the power provided by the sources and gained by the sinks

To investigate the FEEM for different vehicles, a vehicle model is developed specifically for this purpose. It will be used for parameter studies that cause different cost-power functions within the energy management. Resulting energy distribution and operating costs can be analyzed. In addition, the vehicle model will be used in a sensitivity analysis to show the impact of individual costs like the fuel price or the price of a battery per kWh on the cost-power functions and the energy distribution within the same vehicle.

First, the vehicle model is parameterized with data of a real vehicle, which is capable to drive on different energy sources. The vehicle used was a test truck of the publicly funded ENUBA project that examines the feasibility of electrified heavy duty vehicles [5]. This offers the advantage that energy component models can be verified by comparing simulation results with measurements on the real vehicle. In addition, the operating cost of the implemented energy management in the real vehicle will be compared with the operating costs of the FEEM approach.

II. Model Overview

Simulation models of vehicles can be either microscopic or macroscopic. In a microscopic model, the vehicle components are simulated mathematically. The computing time step size is often very small, down to a range of microseconds. For system analysis, such as energy management analysis, macroscopic models are used. The computation time steps are usually 0.1-1s. The vehicle components are modeled by characteristic lines and characteristic maps or by simple calculations [6]. The vehicle described in this paper is a macroscopic model. The characteristic map-based modelling of vehicle components is established for energy management investigations, especially because of the availability of necessary data and high simulation speeds [7].

Overall, a graphical block diagramming implementation of vehicle models is established for research and development. For this purpose MATLAB and SIMULINK is widely used [8]. It was also used to develop the vehicle model described in this paper. Other typical simulation tools are Modelica / Dymola, AVL Cruise, GT-Drive [9].

To examine an energy management strategy, electrical and mechanical energy flows within the vehicle have to be modeled, a possibility to implement and test the energy strategies has to exist and a flexible parameterization must be possible to achieve fast computation time while investigating parameter variations [10]. Verified vehicle component models have to be freely combinable to simulate different powertrains [7]. Therefore, the developed vehicle model is modular and parameterisable. As figure 3 shows, each energy component is a separate sub-model of the vehicle model, which has a defined interface to the energy management. For every time step each energy component expects a request from the FEEM about the amount of electric power to provide or receive. Within the component models, the power requirement from the energy management is satisfied. This is limited by physical boundaries. The control units of the components are not modeled. The time to fulfil the request of the energy management is significantly shorter than the intervals until new requests are provided by the energy management. For each electrical sink the functionality to be fulfilled utilizing the provided electric power is modeled. This is for example propelling the vehicle to a desired velocity or generating the desired temperature in a heater. Within the electrical source models, the operating costs which originate from the power request of the energy management are calculated.

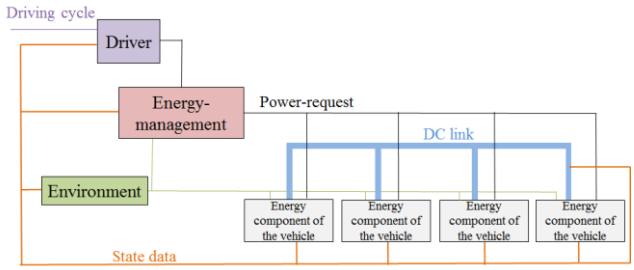

Fig. 3. Overview of the vehicle model

All energy components are connected via the electric DC link, to exchange electric power between sources and sinks. The DC link is physically the DC high voltage backbone in the vehicle. In the model of the electrical circuit, the electric power which the sinks gain is added and subtracted from the sum of the electric power provided by the sources. If the state data of the DC link is zero, the energy balance is ensured.

Environmental data are for example the temperature, air pressure and the gradient angle of the road. The sine of the gradient angle is calculated according to (1) with the difference in altitude Δh and the difference in distance Δs driven within one time step.

$$\sin\alpha = \frac{\Delta h}{\Delta s} \tag{1}$$

The altitude of the path is looked up in a characteristic line, like in a map. The calculation of the distance through the vehicle speed, which is part of the state data of one energy component, takes place in the environment sub-model.

III. Energy Component Models

The energy components which are already implemented are traction, motor-generator unit, ultracapacitors, battery, external power supply and auxiliaries. But the number of energy components can be expanded freely.

In the following, the integration of an energy component in the overall vehicle model is demonstrated. Additionally it is shown how the energy component is modeled, parameterized and verified. This is shown at the traction model. The same procedure was used for the other energy components models, which are summarized in section 3.4. The energy component traction uses data from the driver and the environment and can be a source and sink. Therefore the component is a detailed example.

A. *Traction Model within the Vehicle Model*

Figure 4 shows the interaction between the traction model, the driver model and the energy management. The driver model calculates the acceleration and brake pedal position according to the driving cycle and the current vehicle speed and makes further requests for the auxiliary units. The traction control calculates parameters for the cost-power functions according to the driver input. With all parameterized cost-power functions the energy trade takes place in the energy management and the power requests for each energy component, as well as for the traction model are calculated. In addition, the traction control makes a direct request to the mechanical brake. According to the energy trade, among other power requests, the desired electric power $P_{el,EM}$, that the electric motor should provide or receive, is calculated. Due to the electric power and the current speed of the electric motor n_{EM} a driving or braking torque occurs. This torque generates a force at the wheel according to the gear ratio at the drive axle and the wheel radius. In addition a brake force can act at the wheel depending on the mechanical brake. In the sub model "longitudinal dynamics" there is a balance of forces between the force which arises at the wheel due to the electric motor and the mechanical brake and the driving resistance forces of the vehicle. For the driving resistance the gradient angle of the environment model is considered. Within the longitudinal dynamic model the current vehicle velocity is calculated for the driver model.

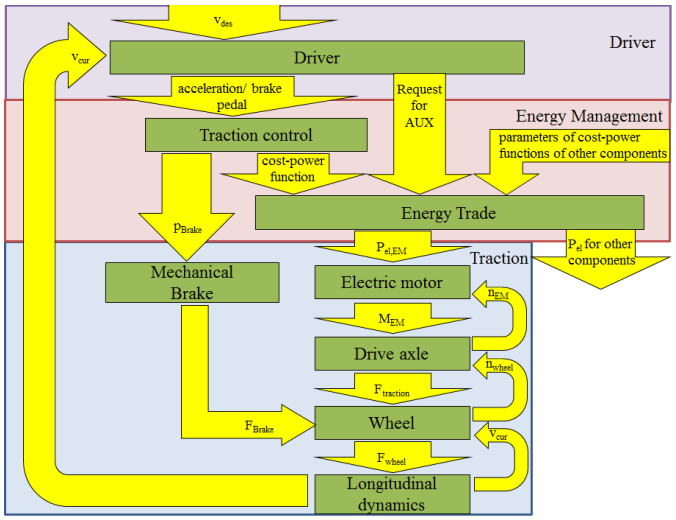

Fig. 4. Energy component traction within the vehicle model

1) Driver Model: The developed vehicle model is a forward-facing longitudinal dynamic model. The relevant part of the driver model for the traction model is a PI controller, that uses the difference between the desired vehicle velocity of the drive cycle v_{des} and the current vehicle speed v_{cur} as the control error [10]. The output of the controller are values between 0 and 100% defining the positions of the acceleration pedal and the brake pedal [10]. Thus, a minimization between desired and current speed of the vehicle is gained by operating the pedals [7]. For the energy management investigation a detailed driver model that differentiates driver-specifically, such as in [12] is not necessary. The influence of the driver to the operating costs will not be examined. But the influence of the energy distribution within the vehicle on the operating costs at a given driving profile and therefore a specific power consumption of the traction will be analyzed. A retarder was not implemented in the driver model as it cannot be generally calculated without developing a driver-individual model, as each driver chooses either the retarder or the brake pedal to his preference to decelerate. However, the traction control is able to consider all driver inputs including the retarder, if the driver inputs are defined instead of a driving cycle.

2) Traction Control Model: To compare the operating costs due to power distribution according to the FEEM in the simulation with operating costs at the real vehicle, the power requirements by the traction should be identically. Therefore, substantial parts of the traction controller of the ELFA drive system, which is a electric traction system of Siemens, were modeled according to the documentation [13] and parametrized with the values that were set in ENUBA truck. In the present state of the model a further brake blending, i.e. dividing the brake power between the traction motor and the mechanical brake, as introduced for the FEEM in [4] is not implemented. The traction controller works in four steps. Some of the functions that are implemented in the control in the real vehicle are not part of the traction control model in the simulation. For example the torque limitations for ASR and ABS and the integration of the crawling gear are not modeled. In addition, backwards driving is not included in the model. These functions have a negligible effect on the operating costs.

In the first step, three characteristic lines corresponding to the acceleration pedal position [%], the brake pedal position [%] and the lever position of the retarder are used to determine the desired proportion of the maximum torque of the traction motor. If the driver does not use the acceleration pedal, a small negative proportion of the motor torque is desired. This represents the drag torque of an engine that drivers of vehicles with internal combustion engines are used to. If both, the brake and acceleration pedals are used at the same time, the brake pedal has a higher priority. The result of the first step is the desired proportion of the maximum torque of the electric motor, which is between -1 (maximum possible braking torque) and +1 (maximum accelerating torque).

The desired proportion of the maximum torque is limited in the second step. First, a speed limitation is performed. Therefore the proportion of the maximum torque is limited at high speeds according to a hysteresis. To prevent high torque gradients and thus to avoid voltage peaks in the intermediate electric circuit, time ramps are introduced. Consequently there is a time limit before the desired proportion of the maximum torque can change significantly. For low engine speeds, the proportion of the desired maximum brake torque is limited along a hysteresis function.

In the third step, the desired torque of the electric motor $M_{des,EM}$ is calculated according to (2) with the proportion of the desired maximum torque $\%M_{max,EM}$, the maximum motor torque $M_{max,EM}$, the rated motor speed $n_{rate,EM}$ and the current motor speed $n_{cur,EM}$. This takes into account that the maximum motor torque decreases in the field weakening range.

$$M_{des,EM} = (\%M_{max,EM}) \frac{n_{rate,EM}}{n_{cur,EM}} M_{max,EM} \qquad (2)$$

In the fourth and last step, the electric power $P_{el,EM}$ is calculated, which is gained by the electric motor or provided by it. The power is calculated using (3) and considering the power loss P_{loss}. The power losses are approximated by using the efficiency map of the electric motor and the efficiency of the power electronics in the vehicle model. The exact calculation of the traction control of the real vehicle is not implemented.

$$P_{el,EM} = (2\pi M_{des,EM} n_{cur,EM}) + P_{loss} \qquad (3)$$

3) Energy Trade: Within the FEEM there are energy components, such as traction, that are both source and sink. Therefore, this energy component has two cost-power functions for the energy trade [4].

If the vehicle should be propelled according to the driver input, the cost-power function of the traction model as a sink is considered for the energy trade. Within the FEEM there are electrical sinks, such as the traction component, that always need to be supplied with electric power, since they are classified with the highest priority [4]. Therefore, it is ensured by the shape of the cost-power function that the energy component gets the electric power according to the driver's request after the energy trade.

During braking, the traction motor acts as a generator and converts mechanical energy into electric energy, which is referred to as regenerative braking [11]. The shape of the cost-power function of the traction component as a source expresses that electric power provided by recuperation is cost free. Therefore, the power provided by the traction component will certainly be gained by the sinks, as all other sources, such as the engine-generator unit, offer electric power for higher prices. In addition, no operating costs occur which have to be modeled in the energy component traction.

B. Traction Model

The traction model consists of the sub models electrical motor, drive axle, mechanical brake, wheel and longitudinal dynamics.

1) Electrical Motor: The bidirectional operation of the electric motor is included in the model, by declaring the drive torque positive, and the brake torque negative. The submodel electric motor consists of three steps. In the first step power limits are ensured. With the maximum torque $M_{max,EM}$ and the current speed $n_{cur,EM}$, the mechanical power limit $P_{mech,max,EM}$ is calculated according to (4) for the base speed range.

$$P_{mech,max,EM} = M_{max,EM} 2\pi n_{cur,EM} \qquad (4)$$

For the field weakening range the power limit is constantly. With the given efficiency of the motor and the power electronics, the maximum electric power is calculated and compared to the request of the energy management. If the desired power is positive, the maximum of the calculated power limit and the power request will be converted to mechanical power. But if the desired power is negative, the minimum of the calculated power limit and the power request will be gained from the mechanical power.

The submodel electrical motor includes the power electronics. Therefore the second step of the electrical motor model describes the power losses at the power electronics with an efficiency η_{PE}.

In the third step, the motor torque, which the electrical motor will provide or receive, is calculated using a characteristic map with the coordinate axis electric power and the current motor speed. This map includes the efficiency of the motor. Consequently, the model of the electric motor represents, as in [1], both, the electrical and the mechanical part, by using a efficiency map, as the specific processes within the electric motor are not important for the energy management.

2) Drive axle: In the submodel drive axle the torque at the wheel caused by the electric motor $M_{wheel,EM}$ is calculated with (5) and the gear ratio i_{DA} and the efficiency η_{DA} throughout the drive train between the traction motor and the wheels [14].

$$M_{wheel,EM} = M_{EM} i_{DA}\, \eta_{DA} \tag{5}$$

The speed of the traction motor n_{EM} is calculated according to (6) with the speed at the wheel n_{wheel} and the gear ratio [14].

$$n_{EM=} n_{wheel} i_{DA} \tag{6}$$

3) Mechanical Brake: In addition to the braking force of the electric motor, operating as a generator, the vehicle model can be decelerated by the mechanical brake. With the driver input through the brake pedal position, the brake torque of the mechanical brake is set. The brake torque is the product of the frictional forces between the brake and the brake disc and the distance between the point of force application and the axis of rotation [16]. Commercial vehicles over 7.5 tonnes gross weight use a compressed air brake to produce the required clamping forces on the wheel brakes [15]. Since it is not necessary for the investigations of the energy management to model the processes in the air brake system in detail, the mechanical brake is simply modeled by a characteristic line, which depicts the correlation between the brake pedal position and the resulting braking force. Overall, the deceleration depends on the performance of the brake system and the static friction between the tires and the road surface [15]. With the characteristic line, however, only the performance of the brake system, but not different friction conditions are modeled.

4) Wheel: Since driving stability aspects are not the focus of the energy management analysis, a simplified one-wheel model can be used [17]. The torque of the electric motor $M_{wheel,EM}$ corresponds to a force with the dynamic tire radius r_{dyn} [18]. In addition to the electric motor, the mechanical brake can apply a negative braking force F_{brake} on the wheel. These forces, combined in (7), are the driving or braking force at the wheel F_{wheel}.

$$F_{wheel} = \frac{M_{wheel,EM}}{r_{dyn}} + F_{Brake} \tag{7}$$

The submodel assumes that the force at the wheel can be transferred to the road and thus (8) is always valid, which means that the axle load F_N multiplied with the adhesion coefficient μ is always smaller than the force at the wheel.

$$F_{wheel} < \mu F_N \tag{8}$$

With the vehicle speed v_{truck}, the wheel speed n_{wheel} is calculated using the dynamic tire radius according to (9) [18]. The tire slip is neglected, as it only has a very small effect on the power requirements of the traction motor of trucks.

$$n_{wheel} = \frac{v_{truck}}{2\pi r_{dyn}} \tag{9}$$

5) Longitudinal Dynamics: With (10) a balance of forces is created at the wheel. The acceleration resistance F_a is equal to the driving respective braking force at the wheel minus the air resistance F_{air}, the rolling resistance F_{Roll} and the gradient resistance F_{grad} [15].

$$F_a = F_{wheel} - F_{Air} - F_{Roll} - F_{grad} \tag{10}$$

By the equation of the acceleration resistance described below, the acceleration or deceleration is calculated. Using the acceleration or deceleration and the speed of the velocity of the previous time step, the current velocity of the vehicle is determined. This is the output of the submodel longitudinal dynamics.

In order to accelerate or decelerate a vehicle, a force must be applied, which overcomes the inertia. Therefore the vehicle must not only accelerate translational, but rotating parts of the vehicle also have to be accelerated. According to (11), the acceleration resistance F_a is calculated with the mass of the vehicle m, the translational acceleration a, and the rotational inertia factor λ [15].

$$F_a = m\lambda a \tag{11}$$

The rotational inertia factor λ is calculated according to (12) with the reduced inertia torque of the rotating parts Θ_{red}, the mass of the vehicle and the dynamic tire radius.

$$\lambda = 1 + \frac{\Theta_{red}}{{r_{dyn}}^2 m} \tag{12}$$

According to (13), the dynamic tire radius is calculated with the rolling circumference U, which is specified for the distance of one turn at a speed of 60 km/h (according to DIN 70020) [15].

$$r_{dyn} = \frac{U}{2\pi} \tag{13}$$

The reduced inertia torque of the rotating parts is calculated according to (14) with the inertia torque of all rotating parts Θ_n , the gear ratio between the observed rotating

part and the wheel, and the inertia torque of the wheels Θ_{wheel} [15].

$$\Theta_{red} = \left(\sum_1^k {i_n}^2\, \Theta_n\right) + \Theta_{wheel} \tag{14}$$

According to [19] the inertia torque of the wheels can be approximated by (15), with the number of tires N_{WH} and the dynamic radius of the wheel. Twin tires are considered as two wheels.

$$\frac{\Theta_{wheel}}{{r_{dyn}}^2} = 56{,}7\ N_{wh} \tag{15}$$

If the vehicle drives upwards a hill or downwards the gradient resistance has to be overcome respectively supports the driving force. It is calculated according to (16) with the proportion of the weight force parallel to the road surface and the gradient angle α [15].

$$F_{grad} = mg\sin\alpha \tag{16}$$

The rolling resistance is calculated in (17) by multiplying the rolling resistance coefficient f_R, that is relatively constant over the speed, and the proportion of the weight force vertical to the road surface [15].

$$F_R = f_R mg\cos\alpha \tag{17}$$

The aerodynamic resistance according to (18) is the product of the density of the air ρ, the drag coefficient c_W, the front surface of the vehicle A_f and the square of the relative velocity of the vehicle speed and the wind speed $v_{truck,rel}$ [15].

$$F_L = \frac{1}{2}\rho c_w A_f v_{truck,rel}^2 \tag{18}$$

C. Traction Model Parametrization

The vehicle model is parameterized to depict a real prototype hybrid truck, the ENUBA truck. This truck is used within a research project with the name ENUBA, which is an acronym standing for electromobility for heavy commercial vehicles to reduce traffic-borne environmental impacts in metropolitan areas.

1) Electric Motor: The electric motor in the ENUBA truck is a permanently excited synchronous machine with a maximum power of 260kW and a maximum torque of 4500Nm. This data is taken into account when limiting the power request of the energy management.

The motor data kindly provided by Siemens include tables that reflect the efficiency of the motor at different speeds and torques for a defined voltage. The voltage in the DC link is usually held to 650V, as the measurements on public roads with the ENUBA truck have shown. Therefore, the characteristic map of the efficiencies at 650V is used in the model.

Figure 5 shows the motor efficiency for different percentages of the maximum mechanical power and at various speeds [20].

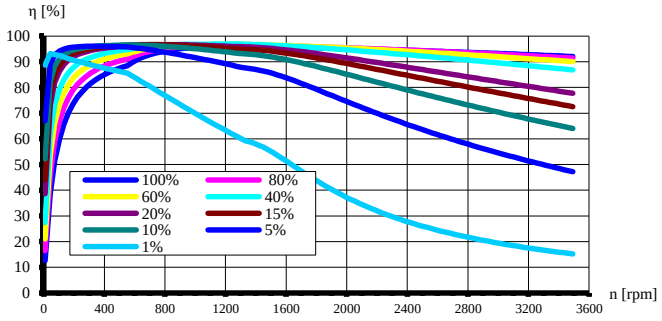

Fig. 5. Efficiency of the electrical motor

To calculate the power limits of the motor, the efficiency at the maximum torque respectively maximum mechanical power and the current speed must be determined. Therefore the efficiency characteristics shown in figure 5 can be used directly in the first step of the motor model.

Within the second step the efficiency of the inverter is assumed with 95%.

To calculate the resulting torque at the given electric power and current speed, in the third step of the model, the efficiency characteristics are typically used as shown in figure 6. By returning the efficiency to calculate the torque an algebraic loop arises. This means that a result of an equation is used as an input of the equation [21]. The problem can be solved by returning the signal with a time delay. But this concludes in the calculation of values, which are no longer entirely accurate.

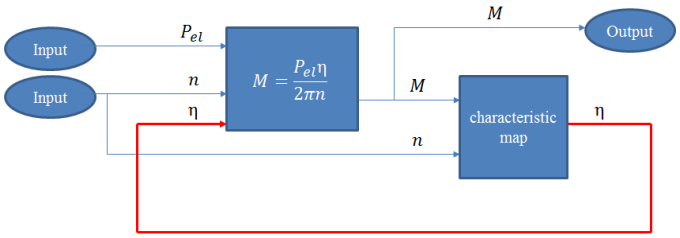

Fig. 6. Algebraic loop at the motor model

To calculate the motor torque directly at a given speed and electric power, the data provided is processed to a characteristic map, which uses the electric power and the current speed as an input to look up the torque and therefore avoid the algebraic loop. For this purpose, the electric power of the motor $P_{el,EM}$ is calculated according to (19) for the given speed and torque of the table provided by Siemens (19).

$$P_{el,EM} = \frac{M_{EM} n_{EM} 2\pi}{\eta_{EM}} \tag{19}$$

For negative torques at a given speed, the same efficiency is assumed as for the absolute value of the torque and the given speed. According to (20) the electric power is calculated for a negative torque.

$$P_{el,EM} = M_{EM} n_{EM} 2\pi\eta_{EM} \quad (20)$$

Thus, the map shown is figure 7 is created. In the characteristic map, the electric power, for example for the maximum torque and the maximum speed is also calculated. In the field weakening range, i.e. at high speeds, the maximum torque is not available. However, this is already considered in the power limits, so that it does not have to be taken into account in this step additionally.

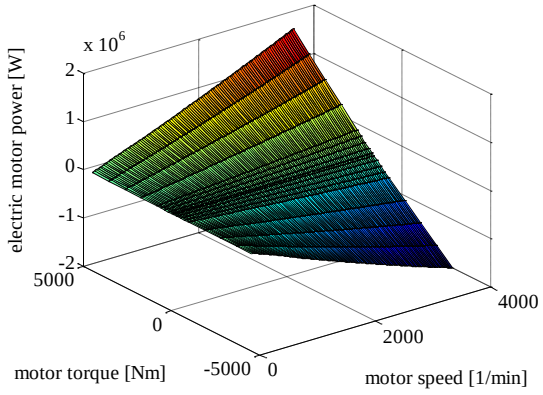

Fig. 7. Electric power of the Motor without field weakening limitation

The characteristic map is then transformed into a new map, which is schematically shown in figure 8. For this purpose, the values of the electric power of the characteristic field are put into a coordinate axis vector and then sorted in ascending order. A new characteristic map is created, with the electric power and motor speed as coordinate axes. Since the map is not complete, the values in the gaps are filled by two dimensional linear interpolations.

	n1	n2	n3
M1	P11	P12	P13
M2	P21	P22	P23
M3	P31	P32	P33

	n1	n2	n3
P11	M1		
P12		M1	
P21	M2		
P13			M1
P31	M3		
P22		M2	
P23			M2
P32	M3		
P33			M3

Fig. 8. Transformation of the characteristic map of the electric motor

2) Drive Axle: In between the electric motor and the wheels are the propeller shaft, the differential, and the drive shafts. There is a constant gear ratio. To determine the gear ratio between the electric motor and the wheels, the vehicle velocity and the speed of the motor was measured. With (6) and (9) and the dynamic tire radius the gear ratio was calculated to $i_{DA} = 6.824$.

According to [22], an efficiency of $\eta_{DA} = 93.5\%$ is assumed for the drive axle.

3) Mechanical Brake: To determine a characteristic line, which depicts the correlation between the brake pedal position and the brake force of the mechanical brake, the brake pedal position was measured via the drive CAN and the brake force was gained on a brake test bench. Since the performance of the test bench is not sufficient to measure high brake forces, the brake force was calculated according to brake tests on the test track. Therefore the brake pedal position is kept constant and the deceleration of the vehicle is recorded. Afterwards the brake force was calculated by the deceleration and consideration of the other driving resistances. The correlation between the brake pedal position and the brake force is shown in figure 9. The maximum brake force of 80 kN is already reached at 50% of the brake pedal position.

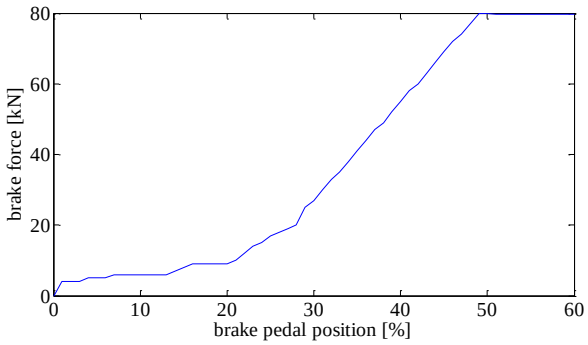

Fig. 9. Correlation of brake pedal position and brake force

4) Wheel: The ENUBA truck uses tires with the size 315/70 R22.5 from Continental. According to [23], they have a circumference of 3090mm. With (13) the dynamic tire radius 0.5m is used in the wheel model.

5) Longitudinal Dynamics: The vehicle mass of 18000kg was determined using a scale. It was not varied during the measurements. The simulation therefore is only parameterized for this mass.

The considered vehicle has two rigid axles, a non-driven, steered front axle and a driven rear axle with a differential gear. In total, as shown in figure 10, the following components need to be rotationally accelerated: an electric motor, a propeller shaft, a differential gear, two driving shafts and four wheels. The wheels at the rear axle have twin tires.

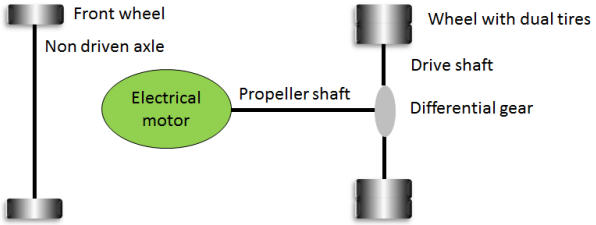

Fig. 10. Drive train of the ENUBA truck

To calculate the reduced inertia torque of the rotating parts of the ENUBA truck (21) is gained from (14).

$$\Theta_{red} = i_{diff}{}^2\,\Theta_{em} + i_{diff}{}^2\,\Theta_{PS} + i_{diff}{}^2\,\Theta_{diff} + i_{AW}{}^2\Theta_{DS} + \Theta_{wheels} \quad (21)$$

With (15) and the permissible neglect of the inertia torque of the propeller shaft Θ_{PS}, the differential Θ_{diff} and the drive shafts Θ_{DS} according to [19] (21) is simplified to (22).

$$\Theta_{red} = {i_{diff}}^2 \, \Theta_{EM} + (56{,}7 N_{wh} \, {r_{dyn}}^2) \qquad (22)$$

With six tires, the inertia torque of the electric motor of 2.4 kg/m² [24], the dynamic tire radius, the vehicle mass, the constant gear ratio and (12) and (22), the rotational inertia factor of the vehicle is $\lambda = 1.04$.

In principle, the rolling resistance and the aerodynamic resistance can be determined individually or at once. If the rolling resistance coefficient is determined individually, a chassis dynamometer is typically used. To determine the drag coefficient, usually tests are carried out in a wind tunnel. To determine the rolling resistance coefficient and the drag coefficient at the same time, for example, due to unavailability of the test benches, coast down tests, towing tests or constant speed tests can be used [18].

In order to determine the rolling resistance coefficient and the drag coefficient the approach of a constant speed test, developed by the TU Graz, which is used for conventional trucks, is applied for the series hybrid ENUBA truck. Within the tests, the traction motor torque, the vehicle speed, the vehicle position and the wind speed are measured. One requirement for the constant speed tests is a sufficiently long and flat route. Additionally, the tires must be filled with the air pressure specified by the manufacturer and be driven for approximately 30 minutes until at desired temperature. The constant speed test is run at the speeds 90km/h, 65km/h, 40km/h and 15 km/h, for at least 20 seconds. During that time at least 20 data sets of the measured data have to be gained [19].

All constant speed tests were carried out on the test track of the ENUBA project. For every speed the constant speed test was run ten times in alternating directions. Additionally, all measurements were carried out with and without the pantograph on the overhead wiring, because different drag coefficients are assumed. The torque was measured at the propeller shaft with strain gauge and directly from the electric motor by reading out the CAN bus. The vehicle position and vehicle speed were measured with an inertial and GPS measurement system. In addition, the wind was measured at half of the distance of the test track with an ultrasonic wind instrument to record the wind speed and wind direction. The height profile of the track with its corresponding GPS data was measured in advance. On the basis of the recorded GPS position in the vehicle and the corresponding height data the gradient resistance was calculated at each measurement time point with (16) and (1).

As it turned out, during the test runs, the measured torque values of the strain gauge at the propeller shaft could not be used, because the battery to supply the strain gauge was also attached to the propeller shaft and broke down at high speeds. Thus, the torque of the motor was used for evaluation. With the measured torque at the electric motor and (5) and (7) the driving force at the wheel was calculated.

The difference of the driving force and the gradient force is, according to (10) at a constant speed, the sum of the rolling resistance and the aerodynamic resistance. The aerodynamic resistance depends on the square of the relative velocity between the vehicle velocity and the wind velocity (18), whereas the rolling resistance is in good approximation independent of the speed (17). Therefore, the parameters x_1 and x_2 of the function in (23) have to be determined in order to calculate the rolling resistance coefficient and the drag coefficient.

$$F_{wheel} - F_{grad} = x_1 {v_{truck,rel}}^2 + x_2 \qquad (23)$$

The relative speed used in (23) is calculated by the difference of the measured vehicle speed and the proportion of the wind speed in driving direction.

Every point in figure 11 is the mean value of one test run. Using the least squares method, a function in the form $y=x_1v^2+x_2$ is approximated. It is shown in figure 11 for the measurements with the pantograph at the overhead wiring.

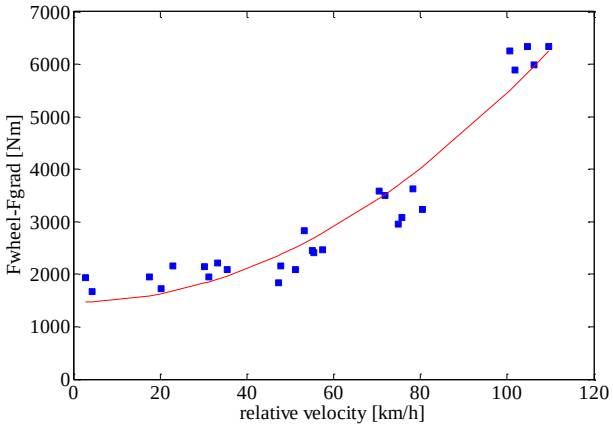

Fig. 11. Sum of rolling resistance and aerodynaimc resistance for relative velocities of vehicle with pantograph at overhead wiring

If x_1 is equal to the rolling resistance, the rolling resistance coefficient is determined according to (17) to $f_r = 0.008$ for the ENUBA truck, both with and without extended pantograph. The parameter x_2 is equal to the air resistance divided by $v_{truck,rel}^2$. The density of the air is assumed to be $\rho = 1.269$, since the measurements were performed at a temperature of 5 °C. The front surface of the vehicle is determined with the program MB-Ruler to $A_f = 9.25\text{m}^2$ without Pantograph and $A_f = 9.83\text{m}^2$ with pantograph. With (18) the drag coefficient results to $c_w = 0.66$ without pantograph and $c_w = 0.82$ with pantograph.

Table 1 summarizes all parameters used in the traction model, besides the characteristic map of the electric motor (figure 5, 7, 8) and the correlation of the brake pedal position and the brake force (figure 9).

TABLE I.

Parameterization of the traction model		
Electric Motor	***Drive Axle / Wheel***	***Longitudinal Dynamics***
$P_{em,mech,max}$ = 260kW	i_{DA} = 6.824	m = 18000kg
$M_{EM,max}$ = 4500Nm	η_{DA}: 0.935	λ = 1.04
η_{PE} = 0.95	r_{dyn} = 0.5	f_r = 0.008
		ρ = 1.269
		A_f = 9.25m² / 9.83m² (without/ with pantograph)
		c_w = 0.66 / 0.82 (without/ with pantograph)

D. Traction Model Verification

Before the traction model is verified, the traction control, which supplies the traction model's inputs, is verified. Afterwards, the calculated driving resistance parameters extracted from the measurements are compared with standard values. With this initial position, the overall traction model is verified by comparing measurements and simulation results for one test drive.

1) Verification of the traction control: In order to verify the simulated traction control, seven trips were recorded at the test site with various possible driver inputs. The recorded driver inputs were used as inputs for the traction control model in the simulation. Thus, the recorded values of the intermediate calculation steps and the results of the traction control in the real vehicle could be compared with the simulation results. To record, a diagnostic tool developed by Siemens, SIADIS, was used. In the first step of the traction control the desired proportion of the maximum torque is calculated according to the accelerating, brake pedal position and lever position of the retarder. As figure 12 shows, the measured data and the simulation results match very good.

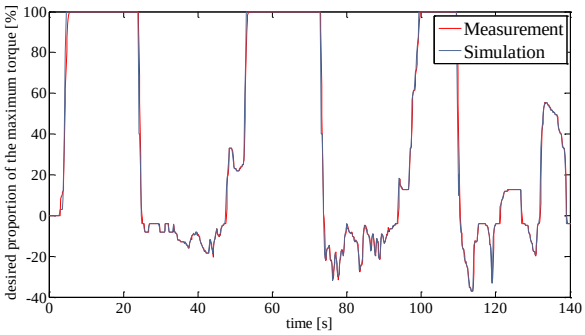

Fig. 12. Comparision of the measurements with the simulation of the desired proportional maximum torque

After limiting the desired proportional maximum torque in the second step the measured data and the simulation results still match, as shown in figure 13. At times when the crawl gear is used, slight deviations are visible, because it was not modeled. Other deviations are due to slightly different measurement time. During the simulation an output is given all 0.2 seconds, whereas the SIADIS stores new values at different points in time.

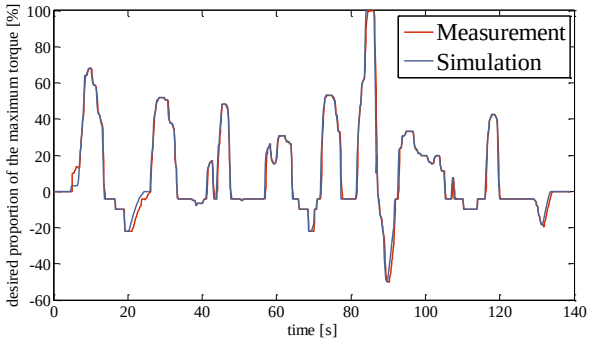

Fig. 13. Comparision of the measurements with the simulation of the desired proportional torque after limiting the torque gradient

With the desired torque determined in the third step, the desired electric power of the electrical motor is calculated in the last step. As shown in figure 14, the measurement of the required power, which can be recorded from the drive CAN-bus, is largely consistent with the simulation result.

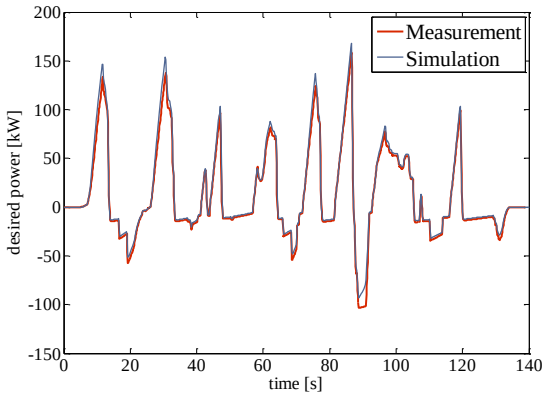

Fig. 14. Comparision of the measurements with the simulation of the desired electric power

Conclusively, it could be demonstrated that the implemented traction control, as part of the energy management, desires the same electric power of the traction motor at the same driver inputs and vehicle velocity as the traction control in the real vehicle.

2) Plausibility check of the driving resistance parameters: Figure 15 shows the rotational inertia factor of conventional trucks [15]. In comparison with a conventional vehicle significantly less parts have to be rotationally accelerated at the series hybrid ENUBA truck. The internal combustion engine, the transmission and possibly a transfer gearbox are not integrated. As can be seen in figure 15, the rotational inertia factor strongly depends on the selected transmission gear between the engine and the wheels. In the ENUBA truck, the ratio is relatively low and constant. Therefore λ = 1.04 is a realistic value.

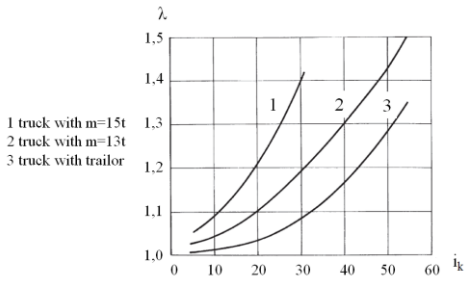

Fig. 15. Rotational inertia factor λ of trucks with the transmission gear i_k [15]

The calculated rolling resistance only applies for a dry sealed surface. However, the rolling resistance may vary with tire pressure, tire temperature or outside temperature. Figure 16 shows typical values of the rolling resistance coefficient on flat roads for trucks with different weights. The calculated rolling resistance coefficient with $f_r = 0.008$ is relatively low, but within the range, for the ENUBA truck with 18kN weight force.

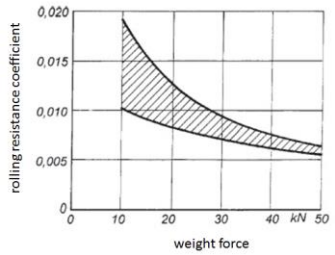

Fig. 16. Rolling fresistance coefficient for trucks [15]

To check the plausibility of the calculated drag coefficients figure 17 shows typical values for various vehicles [15]. The calculated drag coefficient for the ENUBA truck with lowered pantograph is relatively high with $c_w = 0.66$, but within the range.

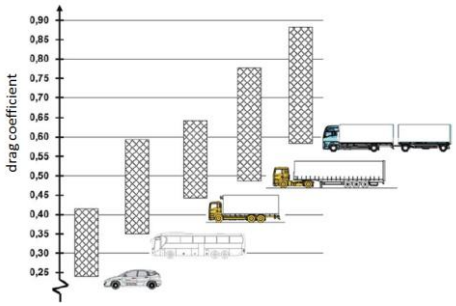

Fig. 17. Aerodynamic drag coefficient for different vehicles [15]

3) Verification of the traction model: In a multi-hour test drive on public roads in and around Berlin (see figure 18) the electric motor power and the brake pedal position was recorded. In addition, the height profile and the vehicle speed were measured. But the wind was not measured while driving.

Fig. 18. Test drive on public roads

The parameterized traction model has the desired measured motor power, brake pedal position and road gradient as an input. The simulated vehicle speed is compared to the measured vehicle speed in figure 19. As the wind was not measured, the air resistance is calculated for the vehicle speed instead of the difference between vehicle speed and the wind speed in driving direction. Since the aerodynamic drag depend quadratic on the relative speed, the deviation of the simulated speed and the measured speed is greater at higher vehicle velocities. The height profile was recorded using GPS. But since the measured height values are often not accurate enough, the calculated gradient force are often not plausible. Therefore, the measured and simulated vehicle velocities mainly match on a road without gradient.

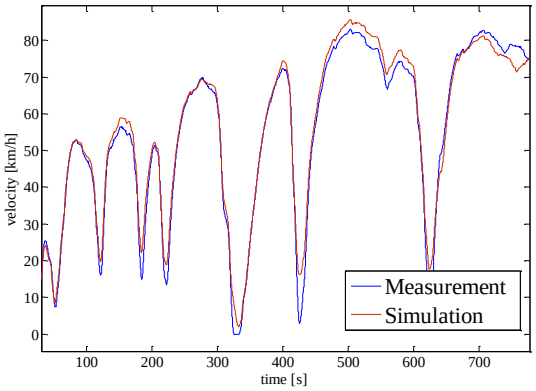

Fig. 19. Comparison of simulated und measured speed for the first 13 min of the test drive

E. Other Component Models

Other energy components are modeled as summarized in Table 2. The table shows the modeling content and the operating costs of sources and sink/sources, which occur next to the maintenance costs.

TABLE II.

Energy Component Models		
Energy Component	***Modeling Content***	***Modeled operating costs***
engine/generator -unit	Specific fuel consumption map (engine), efficiency table (generator)	Fuel consumption
ultracaps	equivalent circuit model	Energy loss due to self-discharge
battery	equivalent circuit model	Replacement caused by aging
external power supply	efficiency	Electricity costs
auxiliary Units	functionality	-

IV. SUMMARY

A vehicle model has been developed to investigate the flexible energy management. For this purpose, energy component models were developed that provide interfaces, which allow easy replacement of components and allow proving the energetic plug-in capability of the energy management. Based on the energy component traction the integration of an energy component within the vehicle model was shown and the method of modelling was demonstrated. The component model was parameterized to demonstrate the components of an existing series hybrid truck, the ENUBA truck. Therefore it was possible to verify the component models. In future work, the operating costs of the flexible energy management will be compared to the energy management of the existing vehicle. Furthermore, a parameter study, to show the variation of the cost-power functions within the energy management for different vehicles as well as a sensitivity analysis, to show the impact of individual costs on the cost-power functions and the energy distribution within the same vehicle, will be performed.

ACKNOWLEDGMENT

Acknowledgments go to the company Siemens, in particular to the department "Technology and Innovation" of the "Mobility and Logistics" division and to the business unit "Rail Electrification" of the "Smart Grid" division for their great support during the measurements to parameterize and verify the vehicle model as part of the ENUBA project. We also would like to thank the business unit "Large Drives" of the "Drive Technologies" division for providing data of the traction control and the electric motor, and Daimler AG at the Truck Product Engineering for providing data to the axis of the vehicle. Further thanks go Alexander Süßmann from the Institute for Automotive Technology at the TU München and to the student Martin Niedermeier who supported the constant speed tests. The project was financially supported by the International Graduate School of Science and Engineering of the TU München. Further acknowledgements go to the Federal Department of Environment (BMUB), which is funding and greatly supporting the ENUBA II project.

REFERENCES

[1] CANDERS: Hybridfahrzeuge und Energiemanagement : Beiträge zum gleichnamigen 1. Braunschweiger Symposium vom 21. Februar 2002, Technische Universität Braunschweig. Als Ms. gedr. Düsseldorf : VDI-Verl., 2002, p. 143, p.29

[2] SPIEGELBERG, Gernot: Ein Beitrag zur Erhöhung der Verkehrssicherheit und Funktionalität von Fahrzeugen unter Einbindung des Antriebstrangmoduls MOTionX-ACT. 1. Aufl. Göttingen : Cuvillier, 2002, pp.44

[3] SCHÖLLMANN, Matthias: Energiemanagement und Bordnetze 2 : Innovative Ansätze für modernes Energiemanagement und zuverlässige Bordnetzarchitekturen. Renningen : expert-Verl, 2007, pp.130

[4] EEHE; HOFF, Carsten (Mitarb.); SIRCH, Ottmar (Mitarb.) : Elektrik, Elektronik in Hybrid- und Elektrofahrzeugen und elektrisches Energiemanagement IV : Mit 57 Tabellen. Renningen : expert-Verl, 2013 (Fachbuch / Haus der Technik 130) , pp. 352- 359

[5] Gerstenberg, Frank; Lehmann, Michael; Zauner, Florian: Elektromobilität bei schweren Nutzfahrzeugen. Munich: eb - Elektrische Bahnen, Volume 110 (2012), issue 8-9, Oldenbourg Industrie Verlag

[6] ADE, Michael: Ein Beitrag zu Modellierung des Antriebsstrangs von Hybrid-Elektrofahrzeugen. Technische Universität Darmstadt, . Dissertation. 2009, pp.19, pp.29

[7] FUGEL, Markus: Parallele Hybridantriebe im Kundenbetrieb. Aachen : Shaker, 2010, pp. 12-22

[8] PROFF, Heike: Zukünftige Entwicklungen in der Mobilität : Betriebswirtschaftliche und technische Aspekte. Wiesbaden : Gabler Verlag, 2012, pp.138

[9] HOFMANN, Peter: Hybridfahrzeuge : Ein alternatives Antriebskonzept für die Zukunft. 1. Aufl. Wien: Springer Wien, 2009, pp.214

[10] BÖCKL, Michael: Adaptives und prädiktives Energiemanagement zur Verbesserung der Effizienz von Hybridfahrzeugen. Düsseldorf : VDI-Verl., 2008, pp.22-35

[11] REIF, Konrad ; NOREIKAT, KarlE ; BORGEEST, Kai: Kraftfahrzeug-Hybridantriebe : Grundlagen, Komponenten, Systeme, Anwendungen. Wiesbaden : Springer Vieweg, 2012, pp.93

[12] GUTTENBERG, Philipp: Der Autarke Hybrid am Prüfstand – Funktion, Kraftstoffverbrauch und energetische Analyse. Technische Universität München, Dissertation. 2004, pp.22, pp.64-65

[13] SIEMENS, Industry Sector, Drive Technologies Division, Large Drives: Functional specification Drive Control Unit for Hybrid Busses powered by ELFA. 14.04.2010

[14] KLEMENT, Werner: Fahrzeuggetriebe. 3. Aufl. München: Hanser, Carl, 2011 (Fahrzeugtechnik), pp.15, pp.20

[15] HOEPKE, Erich: Nutzfahrzeugtechnik: Grundlagen, Systeme, Komponenten. 7., überarb. u. erw. Aufl. 2013. Wiesbaden : Vieweg+Teubner Verlag, 2013, pp.263-277, pp.38-54

[16] REIF, Konrad: Bremsen Und Bremsregelsysteme : Vieweg + Teubner Verlag, 2010, pp. 25

[17] BACK, Michael: Prädiktive Antriebsregelung zum energieoptimalen Betrieb von Hybridfahrzeugen. Karlsruhe : Univ.-Verl. Karlsruhe, 2006 , pp.48-49

[18] HAKEN, Karl-Ludwig: Grundlagen der Kraftfahrzeugtechnik. 2. Aufl. München : Carl Hanser, 2011 (Fahrzeugtechnik) , pp.13, pp.162-167

[19] University of Technology Graz, Institute for Internal Combustion Engines and Thermodynamics “Reduction and Testing of Greenhouse Gas Emissions from Heavy Duty Vehicles -LOT 2” 09 01.2012, pp.22, pp.15-16

[20] Siemens AG, Industry Sector, Drive Technologies Division, Large Drives, interne Untersuchungen

[21] LANGE, Stephan: Energiemanagement in Fahrzeugen mit alternativen Antrieben. Technischen Universität Carolo-Wilhelmina zu Braunschweig, Dissertation. 2007, pp.121

[22] DAIMLER AG, Entwicklung AußenplanetenachsenmTP/ESR, Truck Product Engineering, interne Berechnungen

[23] CONTINENTAL, Technischer Ratgeber Nutzfahrzeugreifen, 2013

[24] SIEMENS AG, Industry Sector, Drive Technologies Division, Large Drives, Berechnungen der Konstruktionsabteilung